PCCP

ROYAL SOCIETY OF CHEMISTRY

PAPER

View Article Online
View Journal | View Issue

Cite this: *Phys. Chem. Chem. Phys.*, 2025, **27**, 1968

State-to-state scattering of highly vibrationally excited NO with argon at collision energies over 1 eV

Chatura Perera,[a] Ethan Ross,[a] Yang Liu,[b] Hua Guo [b] and Arthur G. Suits *[a]

We present state-to-state differential cross sections for rotationally inelastic collisions of vibrationally excited NO $X^2\Pi$ (ν = 9) with Ar using a near-counterpropagating molecular beam geometry. These were obtained using the stimulated emission pumping technique coupled with velocity map imaging. Collision energies well over ~1 eV were achieved and rotational excitations up to $\sim\Delta j$ = 60 recorded for the first time for inelastic collisions. This allowed us to investigate scattering of a diatomic molecule in a $^2\Pi$ state which is initially well described by Hund's case (a) into final states well described by Hund's case (b) as the rotational level splitting becomes larger than the spin–orbit splitting. Differential cross sections for both parity-changing and parity-conserving collisions exhibit very similar structures at the high collision energies. Quantum scattering calculations have been carried out to obtain approximate integral cross sections, which confirm the high rotational excitation. These studies will take the arena of rotationally inelastic collisions to a new regime while providing insight into dynamics under extreme non-equilibrium conditions. Furthermore, these present a unique challenge to both quantum and quasi-classical scattering calculations to validate the methods and the potential energy surfaces used to assess their applicability under extreme conditions.

Received 7th November 2024,
Accepted 14th December 2024

DOI: 10.1039/d4cp04259j

rsc.li/pccp

Introduction

Energy and momentum transfer *via* inelastic collisions are central aspects of chemical dynamics and their study provides a revealing platform for a detailed understanding of molecular interactions. Crossed molecular beam methods represent a powerful tool for gaining deep insight into these processes. One particularly rich domain has been provided by experimental studies on inelastic collisions of diatomic molecules in $^2\Pi$ electronic states with closed-shell targets.[1] Notable experimental advances and recent breakthroughs have been achieved in measuring differential cross sections of these collisions with precise control and resolution of the initial and final quantum states and collision energies down to a few kelvins.[2–4] Parallel advances have also followed in the theoretical understanding of these collisions through the application of quantum scattering calculations on accurate *ab initio* potential energy surfaces.[5,6] Many such systems have been studied including NO($X^2\Pi$), OH($X^2\Pi$), CN($A^2\Pi$), and CaF($A^2\Pi$)[7–13] and a number of general relationships have been derived by a formal quantum analysis.[14] Open-shell species have special appeal in exploring inelastic collisions due to many possible transitions as well as convenient and sensitive detection methods. The interesting internal structure includes spin–orbit and Λ-doublet states which may participate in collisions with rare gases or other molecules. Over the past few decades, collisions between rare gases and nitric oxide (NO) have stood out as the prime example for exploring the detailed dynamics of collisions involving molecules with open-shell configurations.[3,4,6,7] This is both because the NO molecule is an interesting open shell molecule and also because it is a stable radical that can be readily detected using techniques such as resonantly enhanced multiphoton ionization (REMPI) or laser-induced fluorescence (LIF) despite its theoretical complexity.

NO in its ground electronic state has a $1\sigma^2 2\sigma^2 3\sigma^2 4\sigma^2 1\pi^4 5\sigma^2 2\pi^1$ electronic configuration which gives rise to the $^2\Pi$ term. The lowest rotational states of NO($X^2\Pi$) are well described by Hund's case (a) where the projection of the electronic orbital momentum and the spin angular momentum on the internuclear axis couple together. This results in two spin–orbit states with a lower energy $^2\Pi_{1/2}$ state indicated as Ω = 1/2 and the higher energy $^2\Pi_{3/2}$ state with Ω = 3/2. Furthermore, the rotational manifolds that arise from states $^2\Pi_{1/2}$ and $^2\Pi_{3/2}$ are denoted as F_1 and F_2 respectively. Each rotational level further splits into two closely spaced Λ-doublet

[a] *Department of Chemistry, University of Missouri, Columbia, MO 65211, USA. E-mail: suitsa@missouri.edu*
[b] *Department of Chemistry and Chemical Biology, Center for Computational Chemistry, University of New Mexico, Albuquerque, NM 87131, USA*

components that differ in their total parities. This is due to interaction between electronic orbital and rotational angular momenta. The symmetric and antisymmetric combination of the $+\Omega$ and $-\Omega$ wavefunctions are indicated by e Λ-doublet and f Λ-doublet sublevels respectively. The total parity of the Λ-doublet sublevels is then given by $\varepsilon(-1)^{j-1/2}$ where ε is +1 and −1 for e and f, respectively. The f levels are slightly higher in energy than e levels. When a closed shell target approaches, the degeneracy of NO breaks yielding two potential energy surfaces (PESs) of A' or A'' symmetry.[15] The sum potential $(A' + A'')/2$ is said to govern the spin–orbit conserving collisions while the difference potential $(A' - A'')/2$ induces the spin–orbit changing collisions. Studies involving spin–orbit changing collisions are less common due to their low collisional cross sections compared to spin–orbit conserving collisions.[16–18] Furthermore, collisions considering initial and final state parities have been very useful in testing and validating the accuracy of calculated PESs. Parity conserving collisions show multiple peaks in the differential cross sections (DCSs) due to quantum interference between trajectories at two different NO orientation angles which scatters into the same final state.[19] Generally only a single peak is observed in the DCS for parity changing collisions. It is also shown that the inelastic cross sections are unchanged with respect to the e/f labelling of initial and final states for a number of molecules well described in the Hund's case (a) limit.[20,21] In other words, cross sections will be identical for $(j\mathrm{e} \rightarrow j'\mathrm{e})$ and $(j\mathrm{f} \rightarrow j'\mathrm{f})$ and similarly for $(j\mathrm{e} \rightarrow j'\mathrm{f})$ and $(j\mathrm{f} \rightarrow j'\mathrm{e})$. Depending on the symmetric and antisymmetric nature of the electronic wave function with respect to the plane of rotation, Λ-doublet states are also labeled as A' or A''. When rotational level splitting becomes comparable or larger than the spin–orbit coupling constant an intermediate case or Hund's case (b) is more suitable in describing the NO in $^2\Pi$ state.[20] The unpaired electron of NO lies in the plane of rotation in the A' states and perpendicular to that plane in A'' states.[22,23] Dagdigian and co-workers have discussed in detail how e/f symmetry disappears in the high j limit and the observed cross section asymmetry is a quantum mechanical interference effect.[24] This further demonstrates that two potential energy surfaces are necessary in interpreting collisions of molecules in the $^2\Pi$ state with closed shell partners.[10,15,22] Studies have been carried out for species with both singly filled π^1 orbital and triply filled π^3 orbital giving rise to a $^2\Pi$ state.[22,25]

State-to-state studies offer the deepest insight into these and although final state detection is usually straightforward with laser-based probes, initial state preparation is not straightforward. Preparing NO in single quantum states is difficult due to its open-shell character and low rotational constant but essential for a detailed comparison with theories. This is very important in revealing fine quantum effects including resonances and stereodynamics. Using supersonically expanded beams and hexapoles, the Stark effect of NO has been used to achieve greater detail in scattering experiments by preparing NO in its low-field-seeking $j = 0.5$, −f state for stereodynamics investigations.[16,17,19,26,27] Using this, fully quantum state-resolved differential cross sections (DCSs) have been observed for NO–Ar inelastic collisions in a crossed molecular beam experiment over a modest range of collision energies and orientation dependence of the scattering revealed. These results were accompanied by quantum mechanical close-coupling (QMCC) scattering calculations employing coupled-cluster PESs.[19,28] Experiments and QMCC calculations were able to capture the oscillations in the DCSs that appeared in both parity-conserving and parity-changing collisions validating the accuracy of calculated PESs. Stark deceleration has also been further used to reveal rich details in scattering including diffraction oscillations in the DCSs by achieving very narrow velocity spreads for state-selected reactants.[29–31] These oscillations are extremely sensitive to the effective size of the target.

However, all these studies have been focused on inelastic collisions of the vibrational ground level of NO. Even though QMCC calculations successfully reproduced the experimental results, the accuracy of the NO–Ar PESs was largely untested for the NO molecule stretched in high vibrational levels and for low energy collisions that are dominated by the attractive potential. We recently extended such studies to include DCSs for rotationally inelastic and spin–orbit changing collisions of highly vibrationally excited NO (ν = 10) molecules with closed shell partners Ar and Ne, and were able to test the accuracy of both attractive and repulsive parts of both MRCI (multi-reference configuration interaction) and CCSD(T) (coupled cluster singles, doubles, and perturbative triples) PESs using QMCC scattering calculations.[32–37] We utilized the stimulated emission pumping (SEP) technique which was pioneered by Field and coworkers and used by Wodtke and co-workers to prepare NO in highly excited vibrational levels to investigate rovibrational relaxation rates and surface scattering dynamics.[38–40] We applied SEP to prepare NO (ν = 10) in a single rovibrational level in both spin-manifolds coupled with velocity map imaging (VMI) to measure DCSs for inelastic collisions of NO in a near-copropagating (4° crossing angle) crossed beam apparatus. Fully quantum state-resolved state-to-state DCSs were measured for rotationally inelastic collisions of vibrationally excited NO (ν = 10) at a broad range of collision energies well above room temperature down to the cold limit (~2 K), and for spin–orbit conserving and spin–orbit changing collisions.

The utilization of counterpropagating beam geometries in crossed beam experiments is relatively unconventional. In the early 1990s, Henning Meyer successfully employed a counter-propagating pulsed beam scattering technique in pioneering stereodynamics studies to enable measurements of angle-resolved state-specific product distributions using time-of-flight detection of scattered molecules.[41–44] State-to-state inelastic DCSs for NO–Ne and NO–Ar collisions, obtained by combining the Stark deceleration and VMI techniques were later studied using counter-propagating beams by van de Meerakker and co-workers.[45] All the collisions were carried out at collision energies up to ~1300 cm^{-1}. In the current work we present state-to-state DCSs obtained for rotationally inelastic collisions between vibrationally excited NO (ν = 9) and Ar at two very high collision energies ~1 eV utilizing a near-counterpropagating beam geometry. We have recently reported

use of this experimental geometry in a study of spin–orbit changing collisions over a very broad range of collision energies, although that investigation was confined to low j product states.[46] Here we applied the same SEP technique as mentioned above in our recent work in preparing vibrationally excited NO ($\nu = 9$). In this study we obtained DCSs for very high rotational excitation, up to $\sim j = 60$, which has not been reported before for state-to-state scattering.

Experimental methods

The experiments were carried out in our near-copropagating beam scattering apparatus described in detail elsewhere[33,34,36] following some modifications as shown in Fig. 1. This apparatus consists of a dual valve with two piezo actuators within the same valve body. A separate differential region pumped by a separate turbomolecular pump is used to enclose the source region to facilitate the performance of the detection chamber. We altered the apparatus to perform high energy scattering simply by placing an on-axis beam source on the opposite side of the chamber. A single molecular beam valve with a piezo-stack actuator was added in to a new source chamber which is differentially pumped and is separated from the main chamber.[47] This modification allows us to carry out collisions in a near-counterpropagating geometry with an intersection angle of 176° between the two molecular beams. The interaction region is located only 20 cm away from the nozzle of the new molecular beam source. This significantly improved our scattering signal levels and lowered the angular divergence of the beams at the interaction region compared to previous experiments. More detailed information about the apparatus can be found elsewhere.[34,37]

A mixture consisting of 15% NO seeded in H_2 with a backing pressure maintained at 3.5 bar was used to prepare vibrationally excited NO molecules. The supersonically expanded NO beam was introduced into the chamber through a 0.5 mm nozzle in the new pulsed valve. A pure Ar beam with a backing pressure of 9 bar was expanded through the side beam of the dual pulsed valve positioned off axis on the opposite side of the chamber giving an intersection angle of 176° in the crossing region. Both beams were collimated by skimmers with 1 mm aperture which are 2 cm downstream from valve nozzles. All lasers and both valves were operated at 10 Hz and nominal pulse widths of 25 μs and 20 μs were used respectively for NO and Ar beams. SEP lasers which were loosely focused intersected the molecular beam perpendicularly 1 cm upstream from the interaction region to prepare vibrationally excited NO molecules.

Three tunable dye lasers were used in this experiment. SEP was used to prepare NO molecules in single ro-vibrational states: NO molecules in the beam were electronically excited *via* the $R_{11} + Q_{21}(0.5)$ transition of the 2–0 band from the NO $X^2\Pi$ ($\nu = 0$, $\Omega = 0.5$, $j = 0.5$, +e) to the $A^2\Sigma^+$ ($\nu = 2$, $j = 1.5$, F_1) level by the pump laser. The dump laser was then used to prepare vibrationally excited NO molecules in the spin–orbit ground state *via* the $R_{11} + Q_{21}(0.5)$ transition of the 2–9 band by dumping electronically excited NO molecules into the NO $X^2\Pi$ ($\nu = 9$, $\Omega = 0.5$, $j = 0.5$, +e) level. Scattered NO products in the NO $X^2\Pi$ ($\nu = 9$, $\Omega' = 0.5$, N) level due to rotationally inelastic collisions were detected using a (1 + 1) REMPI scheme around 278 nm *via* the 3–9 band of the $A^2\Sigma^+ \leftarrow X^2\Pi$ transition. The ions produced were then focused onto the microchannel plate (MCP) detector coupled to a phosphor screen from our sliced velocity map imaging setup, and the flashes in the phosphor screen were detected by a CCD camera and the positions of the ion spots were centroided and recorded utilizing our NuAcq acquisition software.[48,49] The measured state-to-state differential cross sections (DCSs) were converted from the LAB frame to the COM frame using a Monte Carlo (MC) forward convolution simulation.[33,50]

Theoretical methods

A modified version of the Hibridon package,[51] which includes the vibrational degree of freedom of the diatom,[52] was

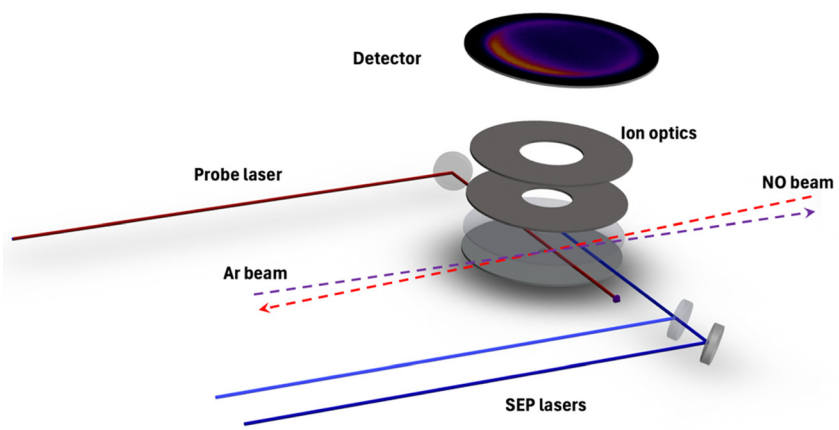

Fig. 1 Schematic of the experimental setup. A molecular beam containing NO in hydrogen, and the other containing pure argon are crossed at an angle of 176°. Scattered products in selected rotational levels of $v = 9$ are detected by (1 + 1) resonance-enhanced multiphoton ionization (REMPI). Corresponding differential cross sections (DCSs) are extracted using the direct current (DC) slice velocity map imaging (VMI) technique.

employed to perform the full-dimensional time-independent quantum scattering calculations using the coupled-states (CS) approximation.[32,33,53,54] Our calculations included three vibrational functions (v = 8, 9, and 10). The collision energy was chosen to be 7100 cm^{-1}. The rotational basis of NO was considered up to j_{max} = 60.5, and the orbital angular momentum was extended to L_{max} = 600.5. The wave function is propagated from 4.2 to 40 bohr. The potential energy surfaces (PESs) used in this work were extended from our previously reported 3D MRCI PESs[32,33] for the $1A'$ and $1A''$ states by adding 4583 additional *ab initio* points calculated at the same level to cover the high energy regions.

An accurate comparison with the measured DCSs is challenging for two reasons. First, an appropriate description of highly excited rotational states of NO needs to follow Hund's case (b), which necessitates a transformation of the basis for NO.[24] Second, the high rotational excitation in the NO product requires a very large basis. We defer the full quantum scattering calculation of the DCS to a future work.

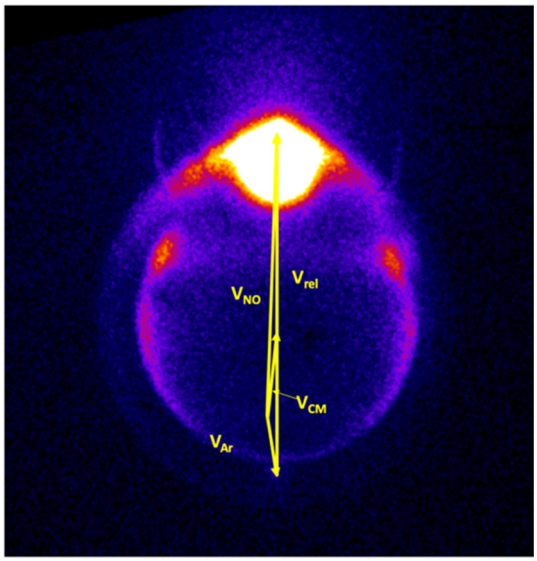

Fig. 2 Newton diagram for the scattering image of NO + Ar at 6800 cm^{-1} collision energy resulting in NO $X^2\Pi_{1/2}$ (v = 9, N = 41, −e), indicating the initial velocities of NO and Ar and the COM velocity.

Results

Here we report fully quantum resolved state-to-state DCSs for rotationally inelastic collisions of vibrationally excited NO (v = 9) and Ar carried out at two hyperthermal collision energies. A collision energy of 6800 cm^{-1} was achieved using a 15% NO beam seeded in H_2 in the center beam and a pure Ar beam as the secondary beam. A velocity of 2480 ms^{-1} for the 15% NO beam seeded in H_2 was obtained. The Ar beam velocity was known from our previous experiments to be 670 ms^{-1}. An example scattering image is shown in Fig. 2 along with the Newton diagram. The initial velocities of NO and Ar as well as the center-of-mass (COM) velocity are indicated in the image. The scattering images presented in here are rotated so that the relative velocity vector is vertical with the NO beam direction toward the top of the figure. There is an intense spot from the NO beam, and forward scattered products from an overlapping transition that is isolated from the distribution of interest in the analysis.

Fig. 3 shows the parity conserving collisions studied at a collision energy of 6800 cm^{-1} (0.84 eV). NO molecules prepared in the $X^2\Pi$ (v = 9, Ω = 0.5, j = 0.5, +e) level following collisions with Ar populate a range of final rotational levels detected using a (1 + 1) REMPI scheme. This initial state of NO is still very much within the description of Hund's case (a). For parity conserving collisions, products were detected in two different rotational levels which are NO $X^2\Pi$ (v = 9, Ω' = 0.5, N = 41, +f) and NO $X^2\Pi$ (v = 9, Ω' = 0.5, N = 53, +f). These will be referred to as 41f and 53f hereafter. Due to the high velocity of the NO beam resulting in high collision energies, relatively high voltages were applied for the electrostatic lenses in the DC slice VMI step up. Voltages of 3000 V, 2648 V, and 2328 V were applied to the repeller, first extractor lens and the second extractor lens. The third extractor lens was grounded. Sufficient statistics for a scattering image were obtained with 300 000 laser shots for a particular rotational level. Images were recorded with 60 000 laser shots and summed together to prevent blurring effects from the valve heating or other variation in experimental conditions. The "raw" experimental center-of-mass DCS was obtained by directly integrating the edge of the scattering image.

As we observed before with near-copropagating beams, a clear symmetry in the scattering image is seen here for near-counterpropagating beams due to the smaller density-to-flux correction compared to a conventional 90° crossing geometry. We have scanned the probe laser delay relative to SEP lasers to capture all the scattered products uniformly during image acquisition. This was necessary to account for the fact that our scattering was not confined to the probe region. The underlying center of mass DCSs were extracted using our previously used Monte-Carlo (MC) simulation code by modifying the code to accommodate the near-counterpropagating geometry. We incorporated all the aspects of the current experiment in this forward-convolution fitting program including measured beam velocity spreads and delays. More details about the fitting program can be found elsewhere.[33] As reported in many previous studies, multiple peaks were observed in the DCSs for both 41f and 53f rotational levels where the parity is conserved.

The parity dependence of these collisions was also studied by probing parity changing collisions at 6800 cm^{-1} as shown in Fig. 4. Here the rotationally inelastic products were detected at NO $X^2\Pi$ (v = 9, Ω' = 0.5, N = 41, −e) and NO $X^2\Pi$ (v = 9, Ω' = 0.5, N = 51, −e). These will be referred to as 41e and 51e hereafter. We have observed multiple peaks in the DCSs for both parity conserving (Δj = odd, e → f) and parity changing (Δj = odd, e → e) collisions in these high collision energy studies involving very high rotational excitations. In contrast, at a collision energy of 530 cm^{-1} we observed only a single main peak for

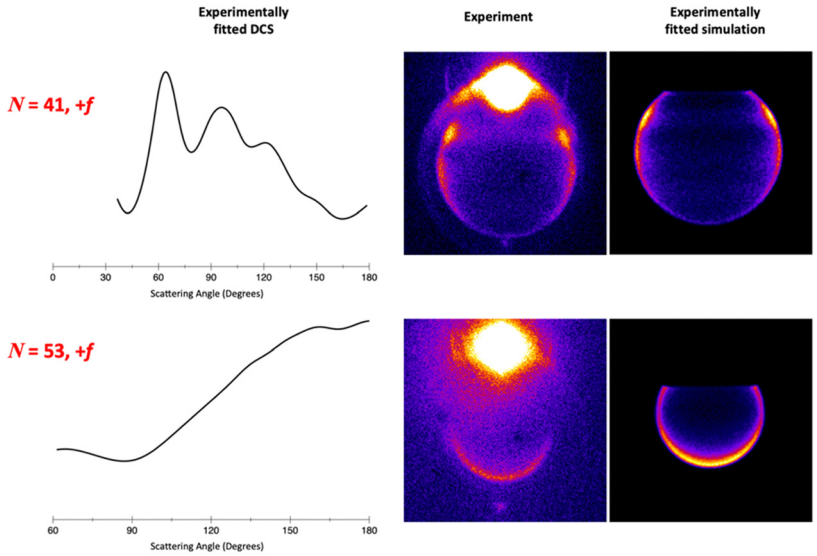

Fig. 3 The experimentally fitted DCS (first column), raw experimental DC slice images (second column) and experimentally fitted DCS image (third column) of the parity conserving inelastic scattering of NO $X^2\Pi$ (v = 9, Ω = 0.5, j = 0.5, +e) with Ar resulting in NO $X^2\Pi$ (v = 9, Ω' = 0.5, N, +f) at 6800 cm^{-1} collision energy.

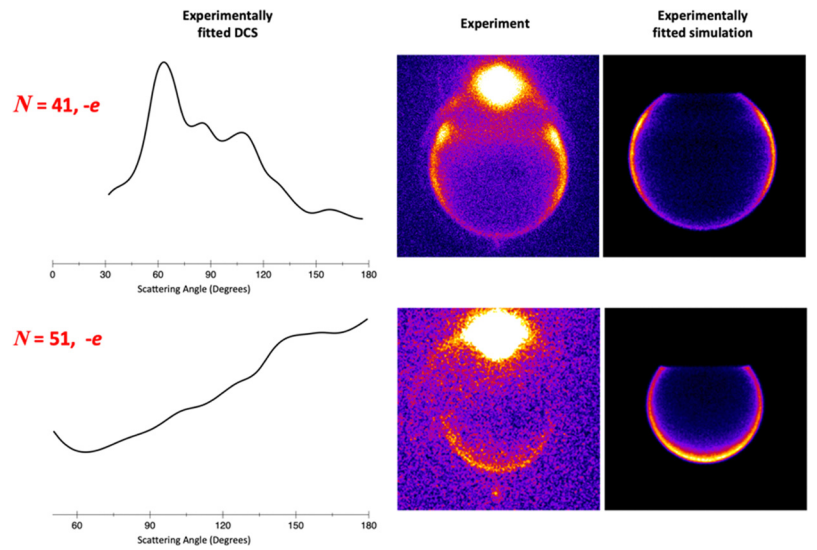

Fig. 4 The experimentally fitted DCS (first column), raw experimental DC slice images (second column) and experimentally fitted DCS image (third column) of the parity changing inelastic scattering of NO $X^2\Pi$ (v = 9, Ω = 0.5, j = 0.5, +e) with Ar resulting in NO $X^2\Pi$ (v = 9, Ω' = 0.5, N, −e) at 6800 cm^{-1} collision energy.

parity changing collisions involving vibrationally excited NO, and this is consistent with the results of Brouard and coworkers for low energy collisions of the vibrationless molecule.[55] In the present high collision energy results, strong sideways scattering peaks are observed at both 41f and 41e. Sideways scattering peaks were shifted to longer scattering angles all the way to backscattered peaks with the increase in rotational excitation up to 53f and 51e at the same collision energy. The reason to study two different final rotational states of 53f and 51e for parity conserving and changing collisions was to avoid overlapping transitions and background due to the amount of available energy at these collision energies and the presence of other vibrational levels populated by spontaneous emission.

A second experiment was carried out at a higher collision energy of 11 200 cm^{-1} (1.4 eV). For this, 15% NO seeded in H_2 collided with a secondary beam which was 15% Ar seeded in H_2. This new gas composition yielded an Ar beam velocity of 1485 ms^{-1}. A new mechanical backing pump had to be used in line with the existing pump to facilitate H_2 pumping and maintain single collision conditions in carrying out these new studies. Here we observed rotational excitations up $\sim\Delta j$ = 60 with the large available energy as shown in Fig. 5.

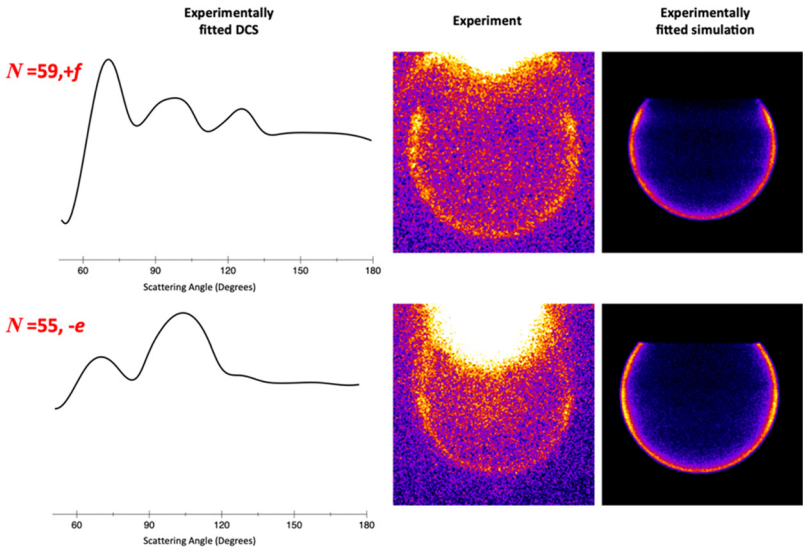

Fig. 5 The experimentally fitted DCS (first column), raw experimental DC slice images (second column) and experimentally fitted DCS image (third column) of the parity conserving (first raw) and parity changing (second raw) inelastic scattering of NO $X^2\Pi$ (v = 9, Ω = 0.5, j = 0.5, +e) with Ar resulting in NO $X^2\Pi$ (v = 9, Ω' = 0.5, N) at 11200 cm^{-1} collision energy.

In this case the rotationally inelastic products were detected at NO $X^2\Pi$ (ν = 9, Ω' = 0.5, N = 59, +f) and NO $X^2\Pi$ (ν = 9, Ω' = 0.5, N = 55, −e). These will be referred to as 59f and 55e hereafter. Energy taken up by the rotational excitation at $\Delta j = 60$ is well over 6000 cm^{-1}. At both collision energies we find both parity-conserving and -changing collisions exhibit multiple peaks in the DCSs.

Discussion

As mentioned in the introduction, the degeneracy of NO breaks when Ar approaches, leading to two PESs of A' or A'' symmetry due to its Π symmetry in the ground state. Spin–orbit conserving collisions are well described by the sum-potential and spin–orbit changing collisions are well described by the difference potential in the pure Hund's case (a) limit. Alexander and co-workers have explained in detail how the molecular wave functions are written in a Hund's case (a) basis with total angular momentum and their projections along space and molecule fixed axes.[12,15] Orbital angular momentum is strongly coupled to the internuclear axis in the Hund's case (a) limit where low rotational states are well described and their collisions extensively studied. The Hund's case (a) scheme breaks down in a few cases. The most relevant scenario happens at highly excited rotational states in which nuclear rotation is so fast that it will lead to the decoupling of the spin angular momentum from the internuclear axis, instead coupling to $\mathbf{N} = \mathbf{\Lambda} + \mathbf{R}$ where $\mathbf{\Lambda}$ is the projection of the orbital angular momentum onto the internuclear axis and $\mathbf{R}$ is the rotational angular momentum. Therefore, in the high j limit Ω is no longer a good quantum number although Λ is. This is because electronic angular momentum is still coupled to the internuclear axis. In other words, Hund's case (a) wave functions are a valid description when the magnitude of the spin–orbit constant A is relatively large in comparison with the product of the rotational constant B and rotational angular momentum $\mathbf{R}$.

An intermediate Hund's case or Hund's case (b) provides a better description outside the above-mentioned limits. Ω = 1/2 and Ω = 3/2 wave functions are mixed by the spin-rotation terms when $A \ll BJ$. In this case the true molecular wave functions are a linear combination of case (a) wave functions. As mentioned before, in case (a), cross sections for ($je \rightarrow j'e$) and ($jf \rightarrow j'f$) will be identical and similarly for ($je \rightarrow j'f$) and ($jf \rightarrow j'e$) independent from the A' or A'' PESs. Therefore, equal populations in the Λ doublet levels for all final states will be observed if an experiment is carried out with equal populations in both Λ doublet levels (e and f) of an initial j. The deviation seen from Hund's case (a) to (b) resulting in unequal final state Λ doublets levels at high j limit even with equal initial Λ doublet levels was studied by Dagdigian and co-workers.[24] They investigated the quantum formalism for scattering of a diatomic molecule in the $^2\Pi$ state which is well described by Hund's case (b). They showed that the differing Λ doublet propensities were due to an interference between the terms in the expansion of the two sum and difference potentials of A' or A'' reflection symmetry. This describes the interaction between a molecule in $^2\Pi$ state and a closed-shell partner. They calculated the cross sections for the CH($X^2\Pi$)–He system at a collision energy of 1000 cm^{-1} and the results were compared with crossed molecular beam studies done by Liu and Macdonald.[56] Furthermore it is also shown that for interaction of a closed-shell partner with a molecule in the $^2\Pi$ electronic state resulting from a singly filled π orbital (π^1) such as CH($X^2\Pi$) and NO($X^2\Pi$), the repulsive interaction will be larger for the A' state. This is

because the π^1 orbital lies in the triatomic plane for the A' state and perpendicular to the triatomic plane for the A'' state. In conclusion the preferentially populated final states are F_1f and F_2e of A'' symmetry whose electronic wave function is antisymmetric.

In this study it is clear that the highly rotationally excited products of vibrationally excited NO with Ar fall closer to the Hund's case (b) limit. By detecting the scattered products in both 41f and 41e at 6800 cm^{-1}, also in 59f and 55e at 11 200 cm^{-1} we have looked at the parity dependence on the DCSs of these collisions involving high rotational excitations. All the studies done so far including our recent work of vibrationally excited NO (ν = 10) have shown multiple peaks in the DCSs for parity conserving (Δj = odd, e → f) and a single peak for parity changing (Δj = odd, e → e) collisions. This was also a confirmation that our initial state preparation by the SEP technique does not populate more than one single rovibrational state. Otherwise, this oscillatory structure would not be resolved if more than a single rovibrational level is populated. Brouard and co-workers observed this product parity sensitivity towards the state-to-state DCS for the NO–Ar system.[19] They utilized a simple four-path hard shell model originally introduced by McCurdy and Miller and extended by Korsch and Schinke to predict quantum interference structures in DCSs and ICSs.[57,58] This model only involves the repulsive part of the PESs which largely governs rotationally inelastic scattering conducted at collision energies corresponding to room temperature or higher. The conclusion of that study was that the parity-conserving DCS is sensitive to both the heteronuclear and homonuclear terms in the interaction potential, whereas the parity-changing collisions are only sensitive to heteronuclear terms. Collisions at two different NO orientation angles interfere to give rise to these oscillations in the DCS as result of homonuclear terms dominating the NO molecule. On the other hand, parity-changing collisions are sensitive only to interferences from different paths involving collisions at the two different ends of the molecule. As NO is a near homonuclear molecule, the phase shifts associated with these different trajectories do not give rise to structures in the DCS at modest collision energies as they are varying slowly. However, in the current study we observe multiple peaks in the DCS for both parity-conserving and parity-changing collisions. This could well be explained by the quantum interferences explained by Dagdigian and co-workers in Hund's case (b).[24] Preferentially populating F_1f could play a critical role as is seen in almost identical scattering signal intensity and features in the DCSs for parity changing collisions. To gain some insight into these processes, we have adapted the four-path model discussed above. Fig. 6 shows the DCSs obtained from the model for both parity-conserving and parity-changing collisions of NO $X^2\Pi$ (ν = 9, Ω = 0.5, j = 0.5, +e) at a collision energy of 6800 cm^{-1} resulting in 41f and 41e. This model also predicts multiple peaks in the DCSs for both parity-conserving and parity-changing collisions, suggesting one aspect of this is more rapidly varying phase shifts at this higher collision energy.

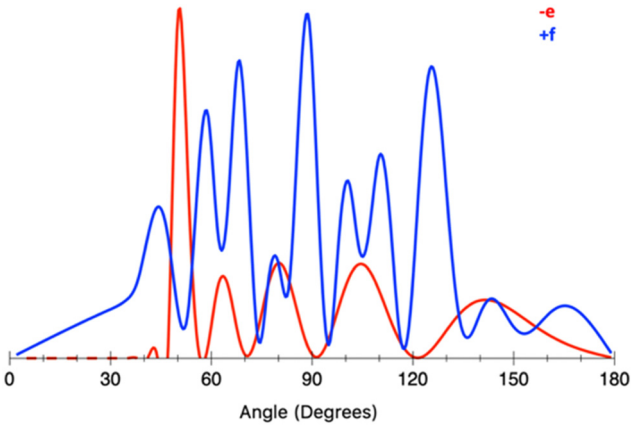

Fig. 6 DCSs from the hard-shell model. Parity conserving (blue) and parity changing (red) inelastic scattering of NO $X^2\Pi$ (ν = 9, Ω = 0.5, j = 0.5, +e) with Ar resulting in NO $X^2\Pi$ (ν = 9, Ω' = 0.5, N = 41) at a collision energy of 6800 cm^{-1}.

Integral cross sections (ICSs) for spin–orbit changing collisions are generally significantly lower compared to spin–orbit conserving collisions.[2,4,16–18] This is mainly due to the fact that the difference potential is smaller than the sum potential. Previous experimental and theoretical work involving rotationally inelastic collisions of spin–orbit changing collisions have shown an increase in the ICS with the increase in rotational excitation ($j_{final} - j_{inital}$) for low Δj transitions. This behavior is in complete contrast with the spin–orbit conserving manifold. Some initial quantum calculations carried out with the CS approximation show the same trend for the studies we have carried out here which involve vibrationally excited NO molecules. Fig. 7 shows the calculated ICSs for both spin–orbit conserving and spin–orbit changing collisions arising from the NO $X^2\Pi$ (ν = 9, Ω'' = 0.5, j'' = 0.5, +e) initial state. These results clearly show the high rotational excitation of the

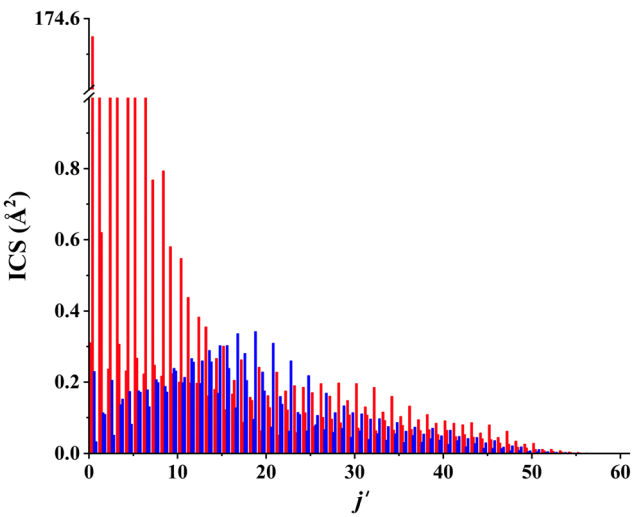

Fig. 7 Calculated ICSs for spin–orbit conserving (red) and spin–orbit changing (blue) collisions arising from the NO $X^2\Pi$ (v = 9, Ω = 0.5, j = 0.5, +e) initial state.

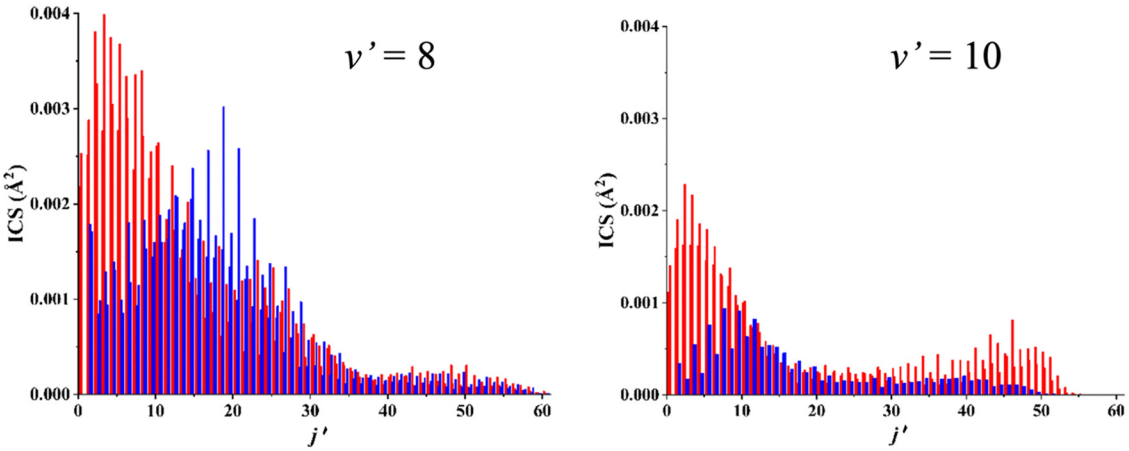

Fig. 8 Calculated ICSs for spin–orbit conserving (red) and spin–orbit changing (blue) collisions arising from the NO $X^2\Pi$ (v = 9, Ω = 0.5, j = 0.5, +e) initial state into the indicated vibrationally inelastic level.

scattered NO. Furthermore, with the increase in rotational excitations for low Δj transitions, the spin–orbit changing collisions show a clear increase in the ICS while spin–orbit conserving collisions show a gradual decrease with the increasing rotational excitation. Fig. 8 shows the ICSs for vibrationally inelastic scattering into v' = 8 and 10. These are lower than the vibrationally elastic cross sections by three to four orders of magnitude. As expected, the exoergic process is favored, in this case by roughly a factor of two.

Conclusions

We have presented velocity map imaging results for rotationally inelastic collisions of quantum state-selected vibrationally excited NO with Ar. Many energy transfer channels including parity conserving and changing collisions were probed. Using a near-counterpropagating molecular beam geometry we were able to achieve collision energies above 1 eV resulting in high rotational excitations, $\Delta j \sim 60$ upon collision, and obtain DCSs for such processes for the first time. Multiple peaks in the DCSs were observed for both parity-conserving and -changing collisions due to this very high rotational excitation. These results can now be used in providing a comparison to quantum and quasi-classical scattering calculations to validate the methods and the potential energy surfaces used to assess their applicability under extreme conditions.

Data availability

Data for this article is available at Zenodo at **https:\\doi.org\10.5281/zenodo.14420606**.

Conflicts of interest

There are no conflicts to declare.

Acknowledgements

This work was supported by the AFOSR program under grant number AFOSR FA9550-22-1-0445 (to AGS), the ARO MURI program under grant number W911NF-1910283 (to AGS and HG) and the Department of Energy (DE-SC0015997 to HG). The quantum scattering calculations were performed at UNM's Center for Advanced Research Computing (CARC).

References

1 R. D. Levine and R. B. Bernstein, *Molecular Reaction Dynamics and Chemical Reactivity*, Oxford University Press, 1987.
2 L. Bontuyan, A. Suits, P. Houston and B. Whitaker, State-resolved differential cross sections for crossed-beam argon-nitric oxide inelastic scattering by direct ion imaging, *J. Phys. Chem.*, 1993, **97**(24), 6342–6350.
3 A. Suits, L. Bontuyan, P. Houston and B. Whitaker, Differential cross sections for state-selected products by direct imaging: Ar^+ NO, *J. Chem. Phys.*, 1992, **96**(11), 8618–8620.
4 H. Kohguchi, T. Suzuki and M. H. Alexander, Fully state-resolved differential cross sections for the inelastic scattering of the open-shell NO molecule by Ar, *Science*, 2001, **294**(5543), 832–834.
5 H. L. Holmes-Ross and W. D. Lawrance, The binding energies of NO–Rg (Rg = He, Ne, Ar) determined by velocity map imaging, *J. Chem. Phys.*, 2011, **135**(1), 014302.
6 H. Cybulski and B. Fernandez, *Ab initio* ground-and excited-state intermolecular potential energy surfaces for the NO–Ne and NO–Ar van der Waals complexes, *J. Phys. Chem. A*, 2012, **116**(27), 7319–7328.
7 K. T. Lorenz, D. W. Chandler, J. W. Barr, W. Chen, G. L. Barnes and J. I. Cline, Direct measurement of the preferred sense of NO rotation after collision with argon, *Science*, 2001, **293**(5537), 2063–2066.
8 G. Parlant and M. Alexander, Trajectory surface-hopping study of electronically inelastic collisions of CN (A 2Π) with

He: Comparison with exact quantum calculations, *J. Chem. Phys.*, 1990, **92**(4), 2287–2295.

9 G. C. Corey and M. H. Alexander, The infinite-order sudden approximation for collisions involving molecules in Π electronic states: A new derivation and calculations of rotationally inelastic cross sections for NO (X 2Π)+ He and Ar, *J. Chem. Phys.*, 1986, **85**(10), 5652–5659.

10 D. Dewangan, D. Flower and M. Alexander, Rotational excitation of OH by para-H/sub 2: rate coefficients calculated in an intermediate coupling representation, *Mon. Not. R. Astron. Soc.*, 1987, **226**(2), 505–512.

11 B. Pouilly and M. H. Alexander, Inelastic collisions of CaF (A 2Π) with He and Ar: Quantum calculations and adiabatic analysis, *J. Chem. Phys.*, 1988, **88**(6), 3581–3589.

12 R. Schinke and P. Andresen, Inelastic collisions of OH (2Π) with H2: Comparison between theory and experiment including rotational, fine structure, and Λ-doublet transitions, *J. Chem. Phys.*, 1984, **81**(12), 5644–5648.

13 B. Nizamov, P. J. Dagdigian and M. H. Alexander, State-resolved rotationally inelastic collisions of highly rotationally excited CN (A 2Π) with helium: Influence of the interaction potential, *J. Chem. Phys.*, 2001, **115**(18), 8393–8402.

14 M. H. Alexander and G. C. Corey, Collision induced transitions between 2Π and 2Σ states of diatomic molecules: Quantum theory and collisional propensity rules, *J. Chem. Phys.*, 1986, **84**(1), 100–113.

15 M. H. Alexander, Quantum treatment of rotationally inelastic collisions involving molecules in II electronic states: New derivation of the coupling potential, *Chem. Phys.*, 1985, **92**(2–3), 337–344.

16 M. Brouard, S. Gordon, B. Nichols, V. Walpole, F. Aoiz and S. Stolte, Differential steric effects in the inelastic scattering of NO (X) + Ar: spin–orbit changing transitions, *Phys. Chem. Chem. Phys.*, 2019, **21**(26), 14173–14185.

17 C. Eyles, M. Brouard, H. Chadwick, F. Aoiz, J. Kłos, A. Gijsbertsen, X. Zhang and S. Stolte, The effect of parity conservation on the spin–orbit conserving and spin–orbit changing differential cross sections for the inelastic scattering of NO (X) by Ar, *Phys. Chem. Chem. Phys.*, 2012, **14**(16), 5420–5439.

18 M. S. Elioff and D. W. Chandler, State-to-state differential cross sections for spin–multiplet-changing collisions of NO (X 2 Π 1/2) with argon, *J. Chem. Phys.*, 2002, **117**(14), 6455–6462.

19 C. Eyles, M. Brouard, C.-H. Yang, J. Kłos, F. Aoiz, A. Gijsbertsen, A. Wiskerke and S. Stolte, Interference structures in the differential cross-sections for inelastic scattering of NO by Ar, *Nat. Chem.*, 2011, **3**(8), 597–602.

20 G. Herzberg, *Molecular spectra and molecular structure: Spectra of diatomic molecules*, Van Nostrand Reinhold, New York, 1950, vol. 1.

21 J. Brown, J. Hougen and K. Huber, IKJWC Johns, H. Lefebvre-Brion, AJ Merer, DA Ramsay, J. Rostas, and RN Zare, *J. Mol. Spectrosc.*, 1975, **55**, 500.

22 R. Dixon and D. Field, Λ-doublet population inversion in collisions of OH, OD, CH, CD and NH^+, *Mon. Not. R. Astron. Soc.*, 1979, **189**(3), 583–591.

23 M. H. Alexander and P. J. Dagdigian, Clarification of the electronic asymmetry in Π-state Λ doublets with some implications for molecular collisions, *J. Chem. Phys.*, 1984, **80**(9), 4325–4332.

24 P. J. Dagdigian, M. H. Alexander and K. Liu, The inelastic scattering of 2Π [case (b)] molecules and an understanding of the differing Λ doublet propensities for molecules of π *vs.* π3 orbital occupancy, *J. Chem. Phys.*, 1989, **91**(2), 839–848.

25 A. Ali and P. J. Dagdigian, Rotational energy transfer within the B 3Πg v = 3 manifold of molecular nitrogen, *J. Chem. Phys.*, 1987, **87**(12), 6915–6926.

26 J. Van Leuken, F. Van Amerom, J. Bulthuis, J. Snijders and S. Stolte, Parity-Resolved Rotationally Inelastic Collisions of Hexapole State-Selected NO (2. PI. 1/2, J = 1/2-) with Ar, *J. Phys. Chem.*, 1995, **99**(42), 15573–15579.

27 A. Gijsbertsen, H. Linnartz, G. Rus, A. Wiskerke, S. Stolte, D. Chandler and J. Kłos, Differential cross sections for collisions of hexapole state-selected NO with He, *J. Chem. Phys.*, 2005, **123**(22), 224305.

28 C. J. Eyles, M. Brouard, H. Chadwick, B. Hornung, B. Nichols, C.-H. Yang, J. Kłos, F. Aoiz, A. Gijsbertsen and A. Wiskerke, Fully Λ-doublet resolved state-to-state differential cross-sections for the inelastic scattering of NO (X) with Ar, *Phys. Chem. Chem. Phys.*, 2012, **14**(16), 5403–5419.

29 A. Von Zastrow, J. Onvlee, S. N. Vogels, G. C. Groenenboom, A. Van Der Avoird and S. Y. Van De Meerakker, State-resolved diffraction oscillations imaged for inelastic collisions of NO radicals with He, Ne and Ar, *Nat. Chem.*, 2014, **6**(3), 216–221.

30 S. N. Vogels, J. Onvlee, S. Chefdeville, A. van der Avoird, G. C. Groenenboom and S. Y. van de Meerakker, Imaging resonances in low-energy NO–He inelastic collisions, *Science*, 2015, **350**(6262), 787–790.

31 J. Onvlee, S. D. Gordon, S. N. Vogels, T. Auth, T. Karman, B. Nichols, A. van der Avoird, G. C. Groenenboom, M. Brouard and S. Y. van de Meerakker, Imaging quantum stereodynamics through Fraunhofer scattering of NO radicals with rare-gas atoms, *Nat. Chem.*, 2017, **9**(3), 226–233.

32 C. Amarasinghe, H. Li, C. A. Perera, M. Besemer, A. van der Avoird, G. C. Groenenboom, C. Xie, H. Guo and A. G. Suits, Differential Cross Sections for State-to-State Collisions of NO(v = 10) in Near-Copropagating Beams, *J. Phys. Chem. Lett.*, 2019, **10**(10), 2422–2427, DOI: **10.1021/acs.jpclett.9b00847**.

33 C. Amarasinghe, H. Li, C. A. Perera, M. Besemer, J. Zuo, C. Xie, A. van der Avoird, G. C. Groenenboom, H. Guo and J. Kłos, *et al.*, State-to-state scattering of highly vibrationally excited NO at broadly tunable energies, *Nat. Chem.*, 2020, **12**(6), 528–534, DOI: **10.1038/s41557-020-0466-8**.

34 C. Amarasinghe, C. A. Perera and A. G. Suits, A versatile molecular beam apparatus for cold/ultracold collisions, *J. Chem. Phys.*, 2020, **152**(18), 184201.

35 C. Amarasinghe, C. A. Perera, H. Li, J. Zuo, M. Besemer, A. van der Avoird, G. C. Groenenboom, H. Guo and A. G. Suits, Collision-induced spin-orbit relaxation of highly

vibrationally excited NO near 1 K, *Nat. Sci.*, 2022, **2**(1), e20210074, DOI: **10.1002/ntls.20210074**.

36 C. A. Perera, J. Zuo, H. Guo and A. G. Suits, Differential Cross Sections for Cold, State-to-State Spin–Orbit Changing Collisions of NO(v = 10) with Neon, *J. Phys. Chem. A*, 2022, **126**(21), 3338–3346, DOI: **10.1021/acs.jpca.2c02698**.

37 C. A. Perera, C. Amarasinghe, H. Guo and A. G. Suits, Cold collisions of hot molecules, *Phys. Chem. Chem. Phys.*, 2023, **25**, 22595–22606, DOI: **10.1039/D3CP02071A**.

38 X. Yang and A. M. Wodtke, Efficient state-specific preparation of highly vibrationally excited NO(X2Π), *J. Chem. Phys.*, 1990, **92**(1), 116–120, DOI: **10.1063/1.458480**.

39 X. Yang, E. H. Kim and A. M. Wodtke, Vibrational energy transfer of very highly vibrationally excited NO, *J. Chem. Phys.*, 1992, **96**(7), 5111–5122, DOI: **10.1063/1.462753**.

40 J. Chen, D. Matsiev, J. D. White, M. Murphy and A. M. Wodtke, Hexapole transport and focusing of vibrationally excited NO molecules prepared by optical pumping, *Chem. Phys.*, 2004, **301**(2), 161–172, DOI: **10.1016/j.chemphys.2004.01.025**.

41 H. Meyer, Electronic fine structure transitions and rotational energy transfer of NO (X 2Π) in collisions with He: A counterpropagating beam study, *J. Chem. Phys.*, 1995, **102**(8), 3151–3168.

42 H. Meyer, Counterpropagating Pulsed Molecular Beam Scattering, *Atomic and Molecular Beams: The State of the Art*, 2001, vol. 2000, pp. 497–518.

43 H. Meyer, Counterpropagating pulsed molecular beam scattering of NH3–Ar. I. State resolved integral cross sections, *J. Chem. Phys.*, 1994, **101**(8), 6686–6696.

44 H. Meyer, Counterpropagating pulsed molecular beam scattering of NH3–Ar. II. State resolved differential cross sections, *J. Chem. Phys.*, 1994, **101**(8), 6697–6707.

45 S. N. Vogels, J. Onvlee, A. von Zastrow, G. C. Groenenboom, A. van der Avoird and S. Y. van de Meerakker, High-resolution imaging of velocity-controlled molecular collisions using counterpropagating beams, *Phys. Rev. Lett.*, 2014, **113**(26), 263202.

46 C. Perera, E. Ross, J. Zou, H. Guo and A. G. Suits, State-to-state spin–orbit changing collision dynamics of vibrationally excited NO at collision energies from 1.4 eV to the cold regime, *J. Phys. Chem. A*, 2024, **128**(49), 10516–10524.

47 C. Abeysekera, B. Joalland, Y. Shi, A. Kamasah, J. M. Oldham and A. G. Suits, Note: A short-pulse high-intensity molecular beam valve based on a piezoelectric stack actuator, *Rev. Sci. Instrum.*, 2014, **85**(11), 116107, DOI: **10.1063/1.4902153**.

48 D. Townsend, M. P. Minitti and A. G. Suits, Direct current slice imaging, *Rev. Sci. Instrum.*, 2003, **74**(4), 2530–2539, DOI: **10.1063/1.1544053**.

49 A. T. J. B. Eppink and D. H. Parker, Velocity map imaging of ions and electrons using electrostatic lenses: Application in photoelectron and photofragment ion imaging of molecular oxygen, *Rev. Sci. Instrum.*, 1997, **68**(9), 3477–3484, DOI: **10.1063/1.1148310**.

50 J. O. F. Thompson, C. Amarasinghe, C. D. Foley, N. Rombes, Z. Gao, S. N. Vogels, S. Y. T. V. D. Meerakker and A. G. Suits, Finite slice analysis (FINA) of sliced and velocity mapped images on a Cartesian grid, *J. Chem. Phys.*, 2017, **147**(7), 074201, DOI: **10.1063/1.4986966**.

51 M. Alexander, P. J. Dagdigian, H.-J. Werner, J. Kłos, B. Desrousseaux, G. Raffy and F. Lique, Hibridon: A program suite for time-independent non-reactive quantum scattering calculations, *Comput. Phys. Commun.*, 2023, **289**, 108761.

52 J. Zuo and H. Guo, Time-independent quantum theory on vibrational inelastic scattering between atoms and open-shell diatomic molecules: applications to NO+ Ar and NO+ H scattering, *J. Chem. Phys.*, 2020, **153**(14), 144306.

53 P. McGuire and D. J. Kouri, Quantum mechanical close coupling approach to molecular collisions. jz-conserving coupled states approximation, *J. Chem. Phys.*, 1974, **60**(6), 2488–2499.

54 R. T. Pack, Space-fixed vs body-fixed axes in atom-diatomic molecule scattering. Sudden approximations, *J. Chem. Phys.*, 1974, **60**(2), 633–639.

55 C. J. Eyles, M. Brouard, C. H. Yang, J. Kłos, F. J. Aoiz, A. Gijsbertsen, A. E. Wiskerke and S. Stolte, Interference structures in the differential cross-sections for inelastic scattering of NO by Ar, *Nat. Chem.*, 2011, **3**(8), 597–602, DOI: **10.1038/nchem.1071**.

56 R. G. Macdonald and K. Liu, State-to-state integral cross sections for the inelastic scattering of CH (X 2Π)+ He: Rotational rainbow and orbital alignment, *J. Chem. Phys.*, 1989, **91**(2), 821–838.

57 C. W. McCurdy and W. H. Miller, Interference effects in rotational state distributions: Propensity and inverse propensity, *J. Chem. Phys.*, 1977, **67**(2), 463–468.

58 H. Korsch and R. Schinke, Rotational rainbows: An IOS study of rotational excitation of hard-shell molecules, *J. Chem. Phys.*, 1981, **75**(8), 3850–3859.